Towards an early 3D-diagnosis of craniofacial asymmetry by computing the accurate midplane: A PCA-based method

Javier Ortún-Terrazas [a,*], Michael J. Fagan [b], Jose Cegoñino [a], Edson Illipronti-Filho [c], Amaya Pérez del Palomar [a]

[a] Group of Biomaterials, Aragon Institute of Engineering Research (I3A), University of Zaragoza, Zaragoza, Spain
[b] Medical and Biological Engineering, School of Engineering and Computer Science, University of Hull, Hull, United Kingdom
[c] School of Dentistry, Department of Orthodontics and Pediatric Dentistry, University of São Paulo, São Paulo, Brazil

ARTICLE INFO

ABSTRACT

Background and objective: Craniofacial asymmetry is a common growth disorder often caused by unilateral chewing. Although an early orthodontic treatment would avoid surgical procedures later in life, the uncertainty of defining the accurate sagittal midplane potentially leads to misdiagnosis and therefore inaccurate orthodontic treatment plans. This novel study aims to 3D-diagnose craniofacial complex malformations in children with unilateral crossbite (UXB) considering a midplane which compensates the asymmetric morphology.

Methods: The sagittal midplane of 20 children, fifteen of whom exhibited UXB, was computed by a PCA-based method which compensates the asymmetry mirroring the 3D models obtained from cone-beam computed tomography data. Once determined, one side of the data was mirrored using the computed midplane to visualize the malformations on the hard and soft tissues by 3D-computing the distances between both halves. Additionally, 31 skull's landmarks were manually placed in each model to study the principal variation modes and the significant differences in the group of subjects with and without UXB through PCA and Mann-Whitney U test analyses respectively.

Results: Morphological 3D-analysis showed pronounced deformities and aesthetic implications for patients with severe asymmetry (jaw deviation > 0.8 mm) in whole craniofacial system, while initial signs of asymmetry were found indistinctly in the mandible or maxilla. We detected significant ($p < 0.05$) malformations for example in mandibular ramus length (0.0086), maxillary palate width (0.0481) and condylar head width (0.0408). Craniofacial malformations increased the landmarks' variability in the group of patients with UXB over the control group requiring 8 variation modes more to define 99% of the sample' variability.

Conclusions: Our findings demonstrated the viability of early diagnosis of craniofacial asymmetry through computing the accurate sagittal midplane which compensates the individual's asymmetrical morphology. Furthermore, this study provides important computational insights into the determination of craniofacial deformities which are caused by UXB, following some empirical findings of previous clinical studies. Hence, this computational approach can be useful for the development of new software in craniofacial surgery or for its use in biomedical research and clinical practice.

1. Introduction

Everyone has some degree of facial asymmetry [1], however, severe asymmetrical growth may cause not only aesthetic but also functional problems [2] which are hardly treated in adulthood, such as temporomandibular joint (TMJ) disorders [2], chephalea [3], malocclusion [4], loss of periodontal support and even loss of teeth [5]. According to Claude Bernard's principle, the development of craniofacial complex is mainly experienced during growth and is conditioned by the paratypic stimulus [6] primarily produced during breathing and chewing [7,8]. Hence, some oral disorders, as mouth breathing syndrome (MBS) [9] or unilateral crossbite (UXB) [10], would be related to the narrowing of the

* Corresponding author at: Aragon Institute of Engineering Research (I3A), School of Engineering and Architecture, University of Zaragoza, Calle María de Luna 3, 50018 Zaragoza, Spain.

E-mail address: javierortun@unizar.es (J. Ortún-Terrazas).

maxilla or the lateral shift of the mandible towards the crossbite side.

Biomechanically, these disorders result in an imbalanced craniofacial complex and therefore, in a potential factor of the asymmetrical growth [11]. Early treatments, such as simple selective grinding or maxilla expander [12], would correct the mechanical imbalance and avoid abnormal irreversible developments and surgical treatments later in life [11,13,14]. Unfortunately, early asymmetry is usually misdiagnosed due to the difficulty of identifying an accurate symmetrical reference which is a key step for pre-treatment evaluation, treatment planning and post-treatment evaluation [15,16]. In 2D-imaging methods, commonly 2D frontal photographs or 2D cephalometric images, the facial midline is estimated through the glabella and other craniofacial landmarks [17] which are generally affected by craniofacial malformations, image's magnifying errors or an inadequate subject posture, among other defects [18,19]. Against these limitations, the progress in imaging acquisition and computer methods has increase the use of 3D imaging techniques [18], such as Computed Tomography (CT), Cone-Beam CT (CBCT) or Magnetic Resonance Imaging (MRI). In this context, CBCT is the most recommended method for an early diagnosis due to its relatively low radiation levels and time required in comparison with the other approaches [20]. Nevertheless, the determination of the appropriate sagittal midplane is still complicated [15,16,21] and the conventional approaches used, such as landmark-based, voxel-based or morphometric midplane approach [21,22], do not compensate the asymmetrical morphology. Among them, the landmark-based method is the most used because it requires just 3 landmarks to define the sagittal midplane [23]. These landmarks are often defined by nasion, crista galli landmarks and cranial base features such as basion [24–26] which are apparently less affected by the facial asymmetry than mandibular ones. Nevertheless, the influence of the facial asymmetry in cranial structures is still unclear and there is no consensus on which landmarks produce more reproducible results [23,27].

Some recent studies [15,16] have proposed robust and easily applicable algorithms, based on Principal Component Analysis (PCA) to determine the accurate plane of symmetry in theoretical cases. In Pinheiro et al. study [16], for instance, the inherent asymmetry of a skull was compensated by mirroring the 3D model through a sagittal midplane defined by PCA. In addition, new approaches [28–30] have been developed to study the asymmetry in superficial soft tissues without a known reference plane for each patient. In Cho et al. study [30], this is achieved through the registration and transformation of a template model with known left and right point correspondences to each scan. Notwithstanding recent advances in 3D imaging and midplane identification methods, these protocols are rarely used in clinical practise and have not been used to diagnose facial asymmetry in real asymmetric patients yet.

The known relationships between malocclusions, as UXB, and asymmetrical malformations are mainly based on statistical 2D studies which used midplanes defined by the inaccurate landmark-based method. The craniofacial malformations are generally analyse [31,32] based on limited number of landmarks through PCA or statistical point distribution models (PDM) [33]. With the advance of 3D imaging techniques, new parametric [34–36] and non-parametric techniques [37,38] have emerged to study the entire shape variability through statistical shape models (SSMs). SSMs describe the shape of a model through the transformation of a template pattern according to its variation modes [39]. Nevertheless, despite the potential of those methods, parametric SSMs require a priori knowledge of the characteristic landmarks which define the shape [38] and non-parametric SSMs require a sufficient number of models to characterize adequately the transformation function [38,40].

Despite the unclear and uncertain relationships, some insights are generally accepted (shown in Fig 1) such as the increase of the mandibular thickness and the condyle of the cross side (XS) [41]. Moreover, there have been reports of an increase in the temporal fossa inclination [42], a reduction of the maxillary width [5,43,44] or the elevation of the ocular orbit and the half cranium [45–48] on the same side. On the other hand, several studies [41,49] agree than the mandibular ramus is longer in the non-cross side (NXS). Contrariwise, some studies did not find a strong correlation between UXB and facial asymmetry and some authors [50,51] even did not find significant differences between the shape of both mandibular halves.

This computational study aims to 3D-diagnose the craniofacial complex malformations that appear in 20 children through 3D cephalometric and midplane identification novel methods. To that end, firstly, the sagittal midplane of 3D models reconstructed from CBCT images was computed compensating the asymmetrical morphology through the mirroring technique and identifying the midplane by PCA. Based on the individual's midplane computed, the variation, differentiation and correlation of several bilateral measurements were statistically analysed by PCA, Mann–Whitney *U* test and Pearson's correlation coefficient, respectively. Deformities in hard and soft tissues were also evaluated by computing the 3D distances between the surfaces of NXS and XS mirrored.

2. Material and methods

2.1. 3D database

CBCT images were obtained from 20 paediatric subjects, fifteen of whom exhibited UXB, (see Table A of the supplementary material) with mixed dentition, which included 9 males (mean age 7.9 years) and 11 females (mean age 8.2 years). According UXB diagnosis, the subjects were classified into 2 groups: a UXB group ($n = 15$) and a control (non-cross bite) group ($n = 5$). The scans of the UXB patients were performed as a part of treatment planning and were classified into 3 categories (minor, moderate and marked) according to the degree of asymmetry by an expert on the diagnosis of facial asymmetry. The control group subjects were scanned for preventive reasons as part of a routine medical examination. The information from the medical images was used exclusively for scientific purposes and was approved by the Research Ethics Committee of the University of São Paulo – USP, School of Dentistry (numbers 200/06 and 16/2008).

All images were obtained with an i-CAT[TM] CBCT imaging system (Imaging Sciences International, Hatfield, PA, USA) with a field of view (FOV) of 13 cm × 17 cm, an acquisition time of 5–26 s and pulse exposure. The images were output in a 14-bit grey scale and 16,384 shades of grey. The focal point was at 0.5 m with a 0.3 mm voxel, an effective dose of 36.74 uSv and cylindrical reconstruction. The data was digitalized by tomography sensors through reconstruction algorithms and converted to the Digital Imaging and Communication in Medicine (DICOM) format. The cylindrical reconstruction of the dataset consisted of 210 images with an interscan distance of 0.50 mm. More details about the scan protocol appear in a previous study [52].

DICOM images were initially filtered by a gradient filter to improve edge definition due to the unmineralized condition of the bones (Fig. 2a). Then, images were segmented by Mimics (Mimics, v.19.; Materialise, Leuven, Belgium) commercial software using threshold levels of 1688 [53] and 226 [54] Hounsfield unit (HU) for dental and osseous regions respectively. The incomplete 3D surfaces (Fig. 2b) were computed through an automated interpolation of the masks. In addition, the cavities of the dental follicles and periodontal ligaments (Fig. 2c and d) were defined through a Boolean subtraction operation with a 0.2 mm [55.56] clearance
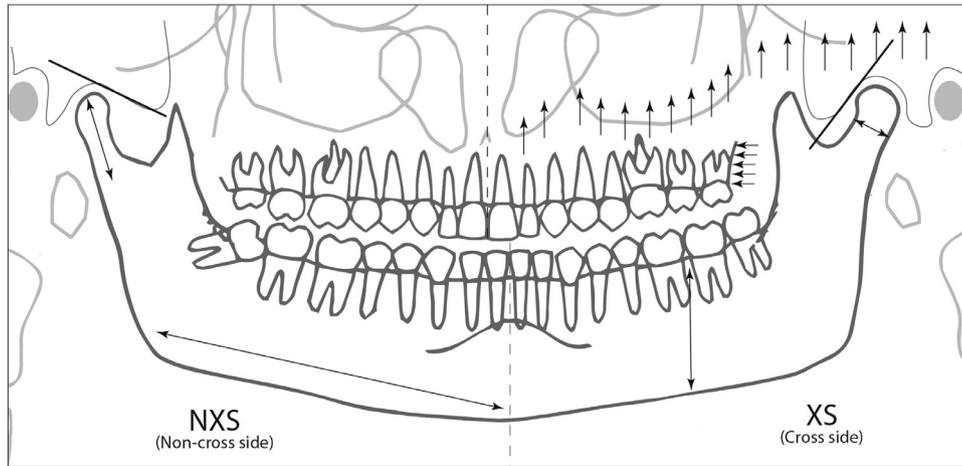
Fig. 1. Panoramic scheme of the morphological changes of the craniofacial complex in a patient with facial asymmetry.
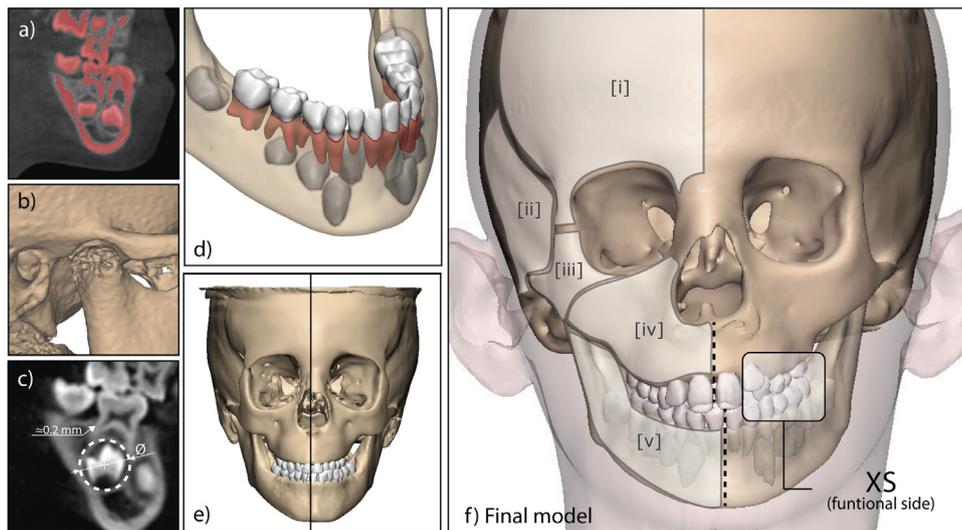
Fig. 2. (a) Small differences between the teeth and the cortical bone; (b) figure showing incomplete regions after automated bone segmentation; (c) approximation of dental follicles and periodontal ligaments as spheres and thin layers around each tooth; (d) detail of the inferior teeth, their periodontal ligaments and the unerupted teeth; (e) left side: model before smoothing operation, right: model after smoothing operation; and (f) model of a patient with UXB in the left side (i: frontal, ii: temporal, iii: zygomatic, iv: maxilla and v: mandible).

around each tooth. The result of the segmentation process is a 3D model composed of the skull, the mandible, the teeth and the superficial soft tissue of the face (Fig 2f). Analytically, each model is a set of N points $\mathcal{P}_N = \{\boldsymbol{p}_i | 1, \ldots, N\}$, where each point i is defined by a vector $\boldsymbol{p}_i = (x_i, y_i, z_i)^T$ in the Cartesian reference system Ω defined by three unitary and orthogonal vectors $\Omega = \{\boldsymbol{i}, \boldsymbol{j}, \boldsymbol{k}\}$. The origin of the reference system was set according to the factory default settings of the i-CAT^{TM} CBCT imaging system. The noise of this point cloud was removed, and the surface was smoothed (Fig. 2e).

For further statistical analyses, thirty-one anthropometric reference points (Table 1) were placed on the hard tissues of 3D models (Fig 3). The soft tissue malformations will not be statistically studied due to the high variance in paediatric patients. The coordinates (x,y,z) of each landmark were reassessed three times by a radiologist expert in the diagnosis of facial asymmetries with a month gap between each assessment. The reliability of this procedure was determined by an Intra-Class Correlation Coefficient (ICC) of 0.91, which was considered enough for the study's scope. From these landmarks, 13 bilateral and 4 global measurements (Table 2) were defined to study statistically the asymmetry. The distance between two landmarks was calculated by the distance formula in

3D coordinate system, while the angle between two vectors was computed by the scalar product of both vectors.

2.2. Size normalization

To reduce the effect of size variations which are inevitable during childhood, the $\mathcal{P}_N$ of the entire volume of each model was uniformly scaled according to the size normalization of the minimum-volume bounding box of the mandible of each patient. The entire volume was not considered to compute the linear transformation matrix T since different cranial portions were scanned for each database. Besides, the minimum-volume oriented bounding boxes approach allows to determine the link among the vertices of the boxes from different patients with different meshes and thus perform the subsequent Generalized Procrustes Analysis (GPA) [57]. Then, a normalization method was developed to equalize the volume of each mandible's set of points, $\mathcal{V}_S$, with the volume of a reference set of points, $\mathcal{U}_R$ (Fig 4a). The reference set was composed by the points of the mandible of third subject (shown in Table A) because he had similar age as the mean age of all subjects and was apparently not affected by the asymmetry. To that end, the minimum-volume oriented bounding boxes (Fig 4b) which contain

Table 1
Definitions of landmarks.

Name	Abbr.	Description
Landmarks on sagittal midplane		
Glabella	G	Most prominent point in the median sagittal plane between the supraorbital ridges
Menton	Me	Most inferior point in symphysis
Pharyngeal tubercle	PhT	Point on the lower surface of the basioccipital region.
Bilateral landmarks (right and left)		
Condyle lateral	CoL	Most lateral point of condyle head
Condyle superior	CoS	Most superior point of condyle head
Gonion	Go	Point between mandibular plane and ramus
Infraorbitale	InfOr	Deepest point on infraorbital margin
Jugale	Ju	Intersection between the margin of the frontal and temporal processes with the zygomatic bone
Last molar	Mo	Most buccal point of the junction between the last molar and the mandible.
Last molar buccal	MoB	Most buccal point of the junction between the last superior molar and the maxilla.
Last molar inferior	MoI	Perpendicular projection of the point on the inferior edge of the jaw.
Last molar lingual	MoL	Most labial point of the junction between the last superior molar and the maxilla.
Porion	Po	Highest point on roof of external auditory meatus
Ramus anterior	RaA	Most posterior point of the intermediate section of the ramus
Ramus posterior	RaP	Most anterior point of the intermediate section of the ramus
Zygion	Zy	Most lateral point of the zygomatic arch
Zygomatic anterior	ZyA	Most anterior point of the intersection between the zygomatic root and the squama of the temporal bone

Table 2
Statistical variables.

Name	Abbr.	Description
Global measurements		
Coronal angle	CoAng	Vertical projection of the angle defined between M plane and sagittal midplane.
Frontal angle	FrAng	Frontal projection of the angle defined between M plane and sagittal midplane.
Mandible deviation	ManDev	Horizontal distance on the FH plane between sagittal midplane and the centre of mass of $\mathcal{V}_S + \mathcal{V}_S^*$.
Menton deviation	MeS	Shortest distance between Me and the sagittal midplane
Bilateral measurements (right and left)		
Body length	Go-Me	Distance between Go and Me
Body width	MoI-Mo	Distance between MoI and Mo
Condylar head height	CoH	Distance of CoS and CoL projections on the S plane
Condylar head width	CoW	Distance of CoS and CoL projections on the FH plane
Gonial angle	GoAng	Angle defined between Go-Me and Go-CoS
Laterality of the gonion	GoS	Shortest distance between Go and the S plane
Laterality of the zygomatic arch	ZyS	Shortest distance between Zy and the S plane
Maxilla height	JuFH	Shortest distance between Ju and the FH plane
Maxilla thickness	MoL-MoB	Distance between MoB and MoL
Maxilla width	MoLS	Shortest distance between MoL and the S plane
Ramus length	Go-CoS	Distance between Go and the CoS
Ramus width	RaA-RaP	Distance between RaA and RaP
Zygomatic arch height	ZyAFH	Shortest distance between ZyA and the FH plane
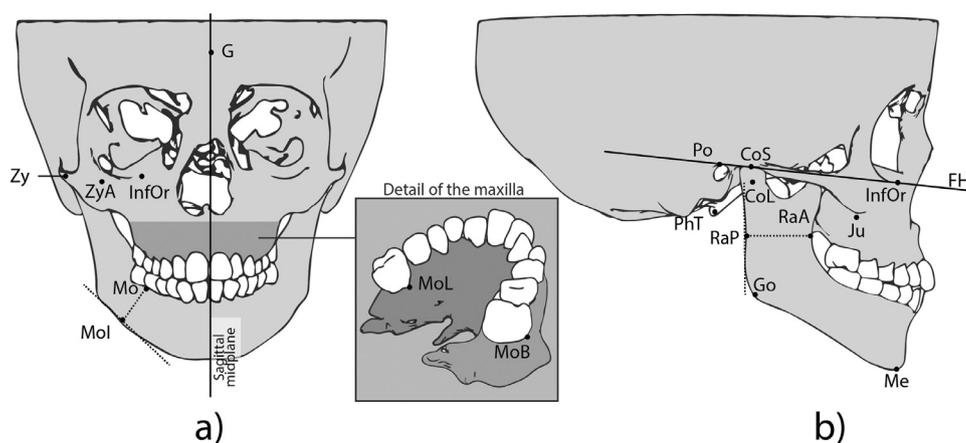
Fig. 3. Landmarks and reference planes in (a) frontal and (b) lateral views of a skull. (Note: Landmarks definitions appear in Table 1).

$\mathcal{V}_S$ and $\mathcal{U}_R$ were computed through O'Rourke's algorithm [58]. The vertices of these boxes were then used to compute the transformation matrix T which transforms $\mathcal{V}_S$ to a set of similar volumes to $\mathcal{U}_R$ through GPA [57] (Fig 4c). As a result of this procedure, the set of points $\mathcal{P}_N$ and of manual-marked landmarks of each subject were scaled by the transformation matrix T.

2.3. Sagittal midplane

For sagittal midplane determination, a computational algorithm [16] which uses interchangeably PCA and Iterative Closest Point (ICP) methods was implemented in the commercial software MATLAB (MATLAB 6.0 R12, The MathWorks Inc, Natick, Massachusetts,
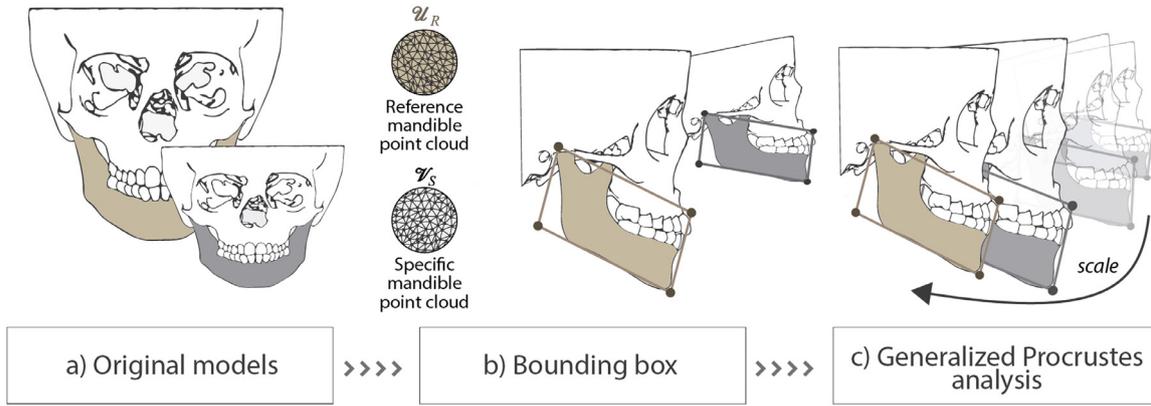
Fig. 4. Scheme of the process followed for the model normalization: (a) Non-scaled models of a specific patient (grey) and the reference subject (brown); (b) minimum-volume oriented bounding boxes of the mandible of each model and (c) linear transformation of the patient model through GPA. (For interpretation of the references to color in this figure legend, the reader is referred to the web version of this article.)
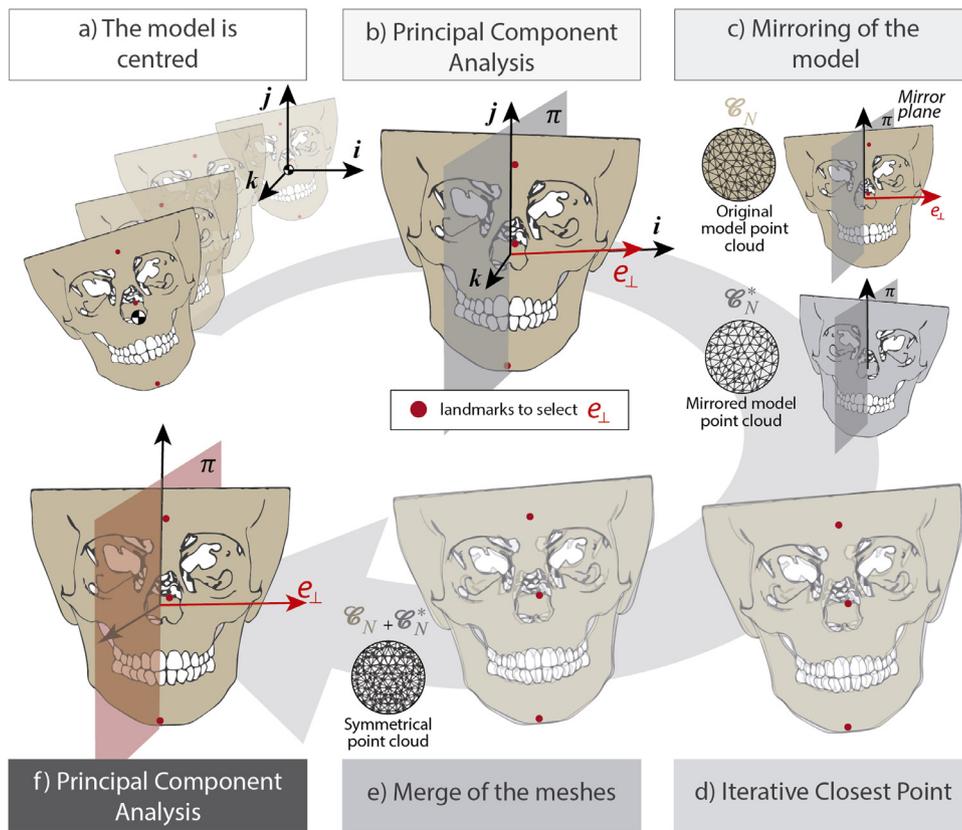
Fig. 5. Flowchart for the identification of the sagittal midplane: (a) the model is centred at the origin of coordinates using its centroid; (b) the initial eigenvectors and a preliminary sagittal plane is computed by PCA; (c) a mirrored model is created from the preliminary sagittal plane; (d) the position of the mirrored set of points is adjusted to the original ones by ICP; (e) both sets of points are merged and (f) the final sagittal midplane is computed by PCA.

2000). This algorithm computes the sagittal midplane of a set of points $\mathcal{C}_N$ which defines the mandible and skull of each patient, compensating for any asymmetric malformation. The PCA technique is widely used to find the eigenvectors e_j that minimize the sum of the projection of each point $p_i \in \mathcal{C}_N$ onto e_i and the squared distances between e_j and p_i. PCA requires firstly that the mean point, o, of the bony structures $\mathcal{C}_N$ is centred to the origin of Ω which is the reference system from which the coordinates of all points are defined (Fig 5a). Therefore, if $\mathcal{C}_N$ is not centred, all points of the model ($\mathcal{P}_N$) and landmarks must be moved through the translation vector v_t defined by the centroid of $\mathcal{C}_N$ as $v_t = (\frac{\sum_{i=1}^{N} x_i}{N}, \ \frac{\sum_{i=1}^{N} y_i}{N}, \ \frac{\sum_{i=1}^{N} z_i}{N})$.

As a result of PCA in $\mathcal{C}_N$, the first three eigenvectors (e_1, e_2, e_3) depend on the portion of skull digitalized and the uniformity of the database. In a uniform set of points of a whole skull, the first principal direction tracks approximately the direction of the line that connects the chin with the parietal bone. Another frequent principal direction is a vector that follows the direction which connects the foramen magnum with the ethmoid bone. Both directions define the sagittal plane that is perpendicular to the undefined principal direction. However, these principal directions are sorted according to the scanned sample. To select the eigenvector that is perpendicular to the sagittal plane $e_\perp$ (Fig 5b) within the principal directions computed, the algorithm employs three hand-

marked landmarks located on the mental protuberance (Me), on the pharyngeal tubercle (PhT) and on the glabella (G), by the procedure explained in Section 2.1. These landmarks define a plane π which is normal to a vector t and apparently parallel to the sagittal midplane searched. Then, the smallest scalar product of each principal directions (e_1, e_2, e_3) with t identifies the $e_\perp$ direction. This direction is used to calculate the rotation matrix Q that aligns $e_\perp$ with the i orthogonal vectors of Ω. The new position of the points is computed by the multiplication of the landmarks and the set of points $\mathcal{P}_N$ by the rotation matrix Q.

To compensate for an individual's asymmetrical morphology, the mirror method was used, as it had already been used in other computational approaches [16,22,59]. This method consists of creating a new set of points $\mathcal{C}_N^*$ symmetrical to $\mathcal{C}_N$ with respect to the sagittal midplane which was previously generated (Fig 5c). Then, $\mathcal{C}_N^*$ is aligned to $\mathcal{C}_N$ by the Iterative Close Points algorithm [60] that minimizes the square of the errors of two sets of points (Fig 5d). The set of points $\mathcal{C}_N + \mathcal{C}_N^*$ represents an idealized symmetrical shape with an equal distribution of points in both halves (Fig 5e). Hence, applying again PCA to the idealized set of points $\mathcal{C}_N + \mathcal{C}_N^*$, (Fig 5f) the eigenvector, $e_\perp$, which is normal to the sagittal plane searched, is obtained by compensating the morphological variations caused by the asymmetry. Finally, the models and their respective landmarks were rotated in that plane to align the horizontal plane with the Frankfort Horizontal (FH) plane, which was defined by the infraorbital and porion landmarks [61], thereby completing alignment of the models.

Although earlier studies have evaluated mandible deviation by the distance between the mental protuberance and the apparent sagittal midplane, the menton location might not be representative of the mandible midplane, as discussed below. Therefore, the algorithm explained previously was also applied only to the set of points that define the mandible $\mathcal{V}_S$, to compute the mandible' midplane, M. The angles between the sagittal midplane of the mandible and of the whole skull were then measured through their projection on to the frontal and coronal planes (global measurements, Table 2).

2.4. Statistical and morphological analyses

The morphological variability in UXB and control groups was analysed for each group by a PDM defined in an open-source code [62] written in Python (Python 2.7.3, Python Software Foundation) for morphometric analysis. The PDM is a statistical analysis which identified holistically the variation of a group of shapes considering the covariation of each point with every other point. The covariance matrix results in a set of eigenvalues and eigenvectors which define respectively the variation level and direction in which the landmarks tend to vary as a group. Sorting the eigenvectors, or modes of variation, in descending order of their eigenvalues, the most representative modes of variation of the thirty landmarks were obtained.

PCA can then be applied by ordering the eigenvectors, and retaining only the modes with the highest values, which represent the modes of variation that account for most of the variation seen in the training shapes. Each PDM consist therefore of a mean shape and principal variation modes whose variation is controlled by their eigenvalues (i.e. ±3 SD). Statistically, the differences between the 17 bilateral measurements of both halves were tested by a Mann-Whitney U test (significance level $P \leq 0.05$). Pearson's correlation coefficient, r, and its associated p-value were also computed to establish the different associations that could be presented between the bilateral and global variables of both groups and halves. All statistical analyses were performed using SPSS software (SPSS software, v. 16.0; SPSS Inc., Chicago, IL).

For 3D evaluation of asymmetric malformations, each 3D model was divided according to the symmetrical midplane previously defined and the left side (cross side in patients with UXB) was mirrored. The normal distance between both halves was then computed in MATLAB and plotted in Paraview software (Paraview v5.6, National Technology & Engineering Solutions of Sandia, New Mexico) to 3D evaluate the morphological differences between both facial sides.

3. Results

PDMs were generated within UXB and control group to define s variability. According to PDMs description, over 95% of the total landmarks' variability in the control and UXB groups is described by 5 and 11 principal variation modes, respectively (Fig 6a and b). The accumulative vector of the first five modes of variation (at −3 SD) in both groups is shown in Figs. 6c and d. While the variation of the landmarks' position was lower in UXB than in the control group, it was also more asymmetric. Alternatively, the landmarks variability for the first five modes of variation is displayed in the supplementary video.

From the statistical analysis, significant differences in the bilateral measurements of condylar head width (CoW), gonial angle (GoAng), ramus length (Go-CoS), maxilla height (JuFH), maxilla width (MoLS) and laterality of the zygomatic arch (ZyS) were found between the XS and NXS data for the UXB group of subjects (Fig 7). The distances measured in XS were greater for CoW and GoAng measurements compared to NXS, and shorter in Go-CoS, MoLS and ZyS. Moreover, the condyloid process width (CoH) and mandible body length (Go-Me) were shorter in XS, although they were not significantly different. Distances of JuFH were significantly greater in NXS than in XS which reflects a deeper position of the jugale landmark (Ju) with respect to the FH plane. Meanwhile, no significant differences were observed between the measurements of both sides in the control group.

From the comparison of the 2 groups (numerical results in Table B2 of the Supplementary material), the differences of the measurements were computed as the difference between the values of both halves, NXS-XS and Right-Left for UXB and control groups respectively. According to our findings, no significant differences were observed for the CoW and ZyS measurements in both groups (Fig 8). Differences in the measurements of GoAng, Go-CoS, JuFH, MoLS, laterality of the gonion (GoS) and ramus width (RaA-RaP) were significantly greater in the UXB group than in the control group. Nevertheless, no significative difference was found between the body width (MoI-Mo) of both groups. Interestingly, for those subjects with UXB, mandible deviation (ManDev) was more significative for UXB diagnoses than the conventional measurement of menton deviation (MeS).

The relationship between the 17 variables in XS, NXS and in the control group are displayed in Fig 9a and b (numerical data summarized in Tables C1-C3 of the Supplementary material). There was a significant positive relationship between the CoW and CoH measurements of the control group and in the NXS side of patients with UXB, but not on the XS. Moreover, a positive and significant correlation was found between Go-CoS and mandible body length (Go-ME) in the control group. On the other hand, the deviation in mandible position (ManDev) was closely related to the reduction of MoLS in XS of the UXB group.

Images a-d in Fig 10 show plots of the normal distance between the surfaces of NXS and XS mirrored through the sagittal midplane in four subjects. The positive (red) areas show where NXS protrudes, while the negative (blue) areas indicate protrusion of XS. The scatter plot in Fig 10e illustrates the positive relationship between the differences of the MoLS and ManDev measurements of both halves in UXB and in the control groups. Using the
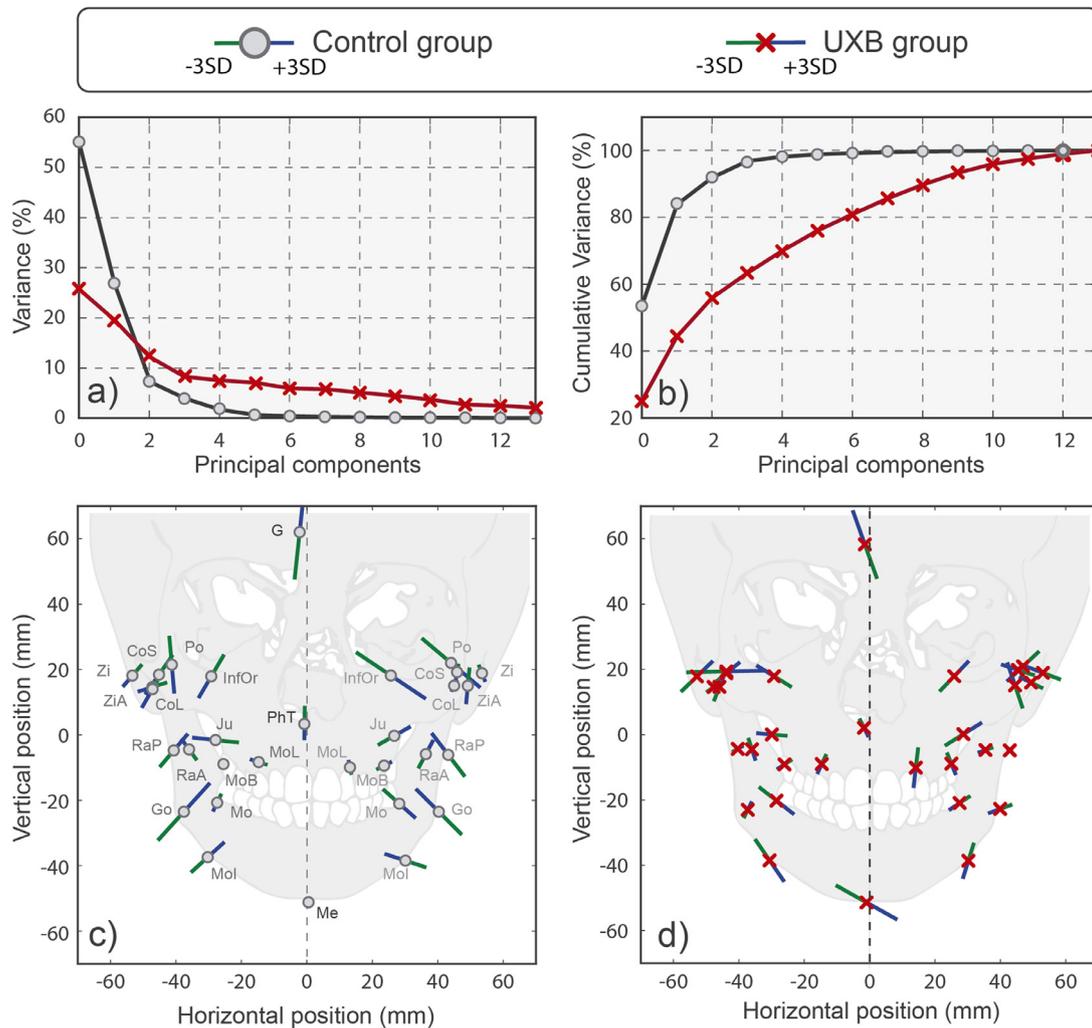
Fig. 6. (a) Percentage and (b) accumulative percentage of landmarks variance described by the principal variation modes. Bottom figures: total vector of the five main modes of variation (at ±3 SD) in the c) control and d) UXB groups.

classification of subjects according to the asymmetry severity (Table A1 of the supplementary material), Fig 10e was divided into 3 regions: minor, moderate and marked asymmetric patients. The minor asymmetric category (Fig 10a) was composed of subjects with short mandible deviation (<0.3 mm) and small differences in MoLS between both sides (±1.5 mm). The moderate asymmetrical subjects mainly presented 2 different malformations, either in the maxilla (Fig 10b) or in the mandible (Fig 10c), which can be differentiated through ManDev and MoLS values respectively. In the first group, the maxilla portion of the XS was less open and slightly higher than those of the NXS, which was also apparent in the cheeks of the superficial soft tissue. Meanwhile, half of the mandible of NXS was more open and longer (Fig 10c) in the case of subjects with mandible malformation. Finally, subjects with marked asymmetry show both maxilla and mandible deformities with a pronounced effect in the superficial soft tissue.

4. Discussion

Although 2D diagnostic tools have been widely used to diagnose asymmetry, their usefulness and associate concepts are recently being questioned because of the high variability, inconsistency and errors during image capture or landmark identification. To solve these limitations [63,64], the use of 3D cephalometric methods, specially CBCT, has increased in the last decade. Never-

theless, the improvement of 3D methods has not demonstrated yet and some studies [65,66]] have not even found significant differences between 2D and 3D methods. Normal approaches to define the midplane, do not compensate the asymmetric shape [67,68] and often use landmarks from areas which could be affected by the asymmetry [48,69], such as the cranial base region, possibly leading to misdiagnosis and inaccurate orthodontic treatments plans. Meanwhile, new methods [28–30] which do not require a specific sagittal midplane have recently been developed to study the asymmetry in soft tissues. As it was introduced, these techniques transform a template model to each model through known landmarks that define its shape. Nevertheless, despite the great potential of these methods, they are hardly applicable in the study of the asymmetry in irregular craniofacial structures because of the unknowledge of the landmarks that define their shape. On the other hand, the use of ionising CT scans and the continually changing state of paediatric bones makes 3D studies difficult in early years. Due to the uncertainties in the sagittal midplane determination and in the development of 3D models of children's craniofacial complex, the relationship between malocclusion and the asymmetric growth of the craniofacial complex is still unclear [70]. This lack of knowledge has complicated the early identification of the asymmetry and therefore its early treatment which is crucial to avoid irreversible abnormal developments [11,13,14].
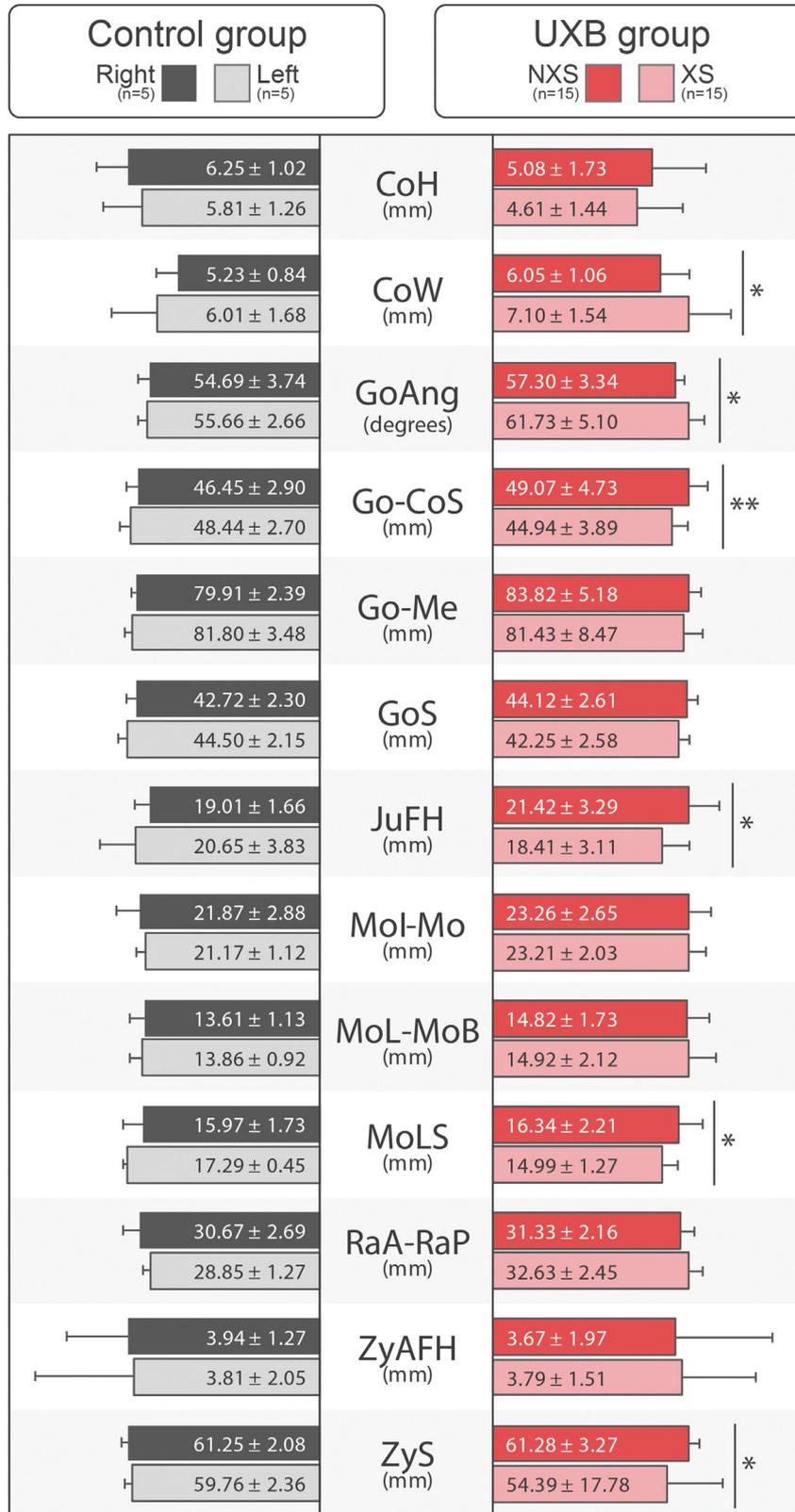
Fig. 7. Bar chart showing the mean ± SD values of the 13 bilateral variables measured in the control group (left) and in the UXB group (right). Significant difference at $p < 0.05$ (*); $p < 0.01$ (**).
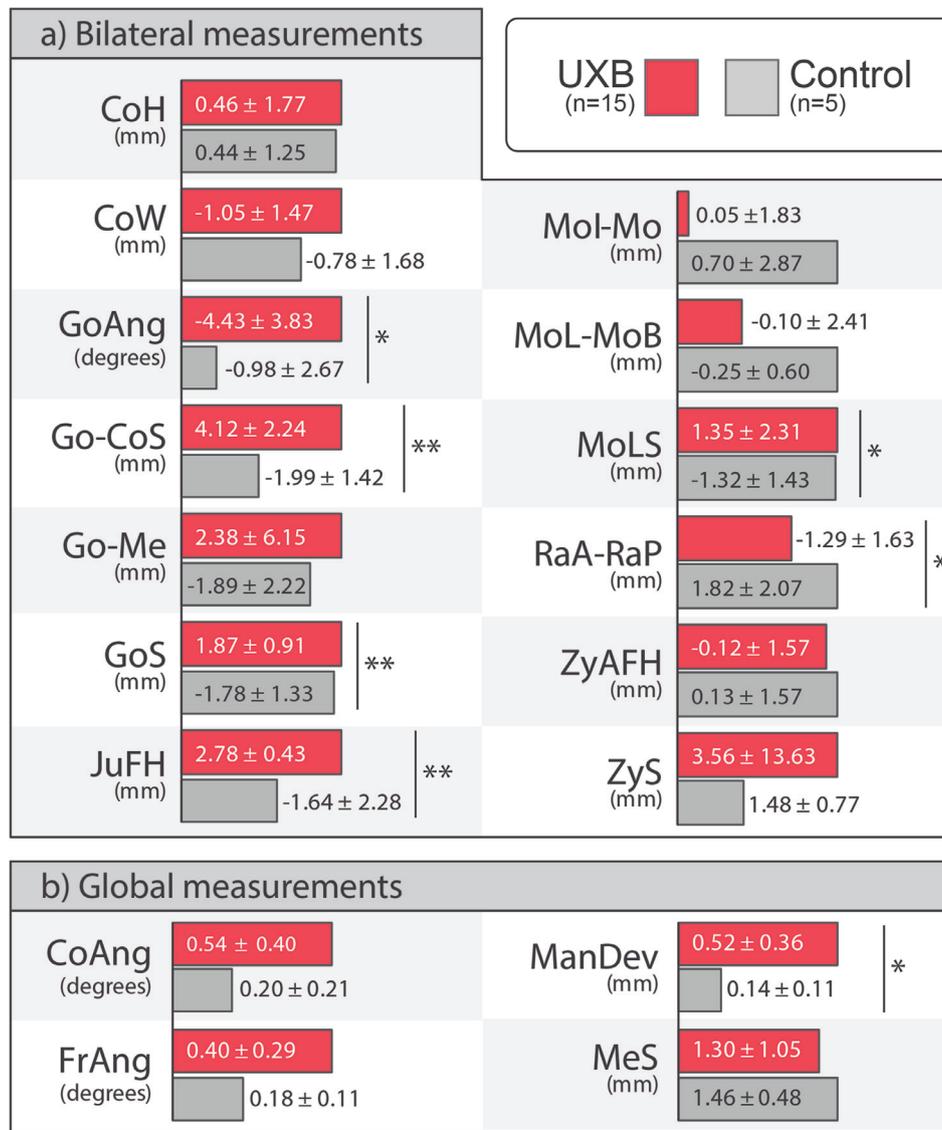
Fig. 8. Bar chart showing the mean value of (a) the difference between the measurements of both sides and (b) global measurements in the UXB group (red bars) and in the control group (grey bars). Significant difference at $p < 0.05$ (*); $p < 0.01$ (**). (For interpretation of the references to color in this figure legend, the reader is referred to the web version of this article.)

In this computational study, the early diagnosis of asymmetrical development in 20 paediatric subjects was 3D-evaluated through CBCT images reconstruction and the accurate identification of the sagittal midplane by a PCA-based method. Although this method was recently demonstrated and validated in a theoretical case of an induced growth pattern of a single skull [16], until now, it had not been evaluated in real paediatric patients with facial asymmetry. For the 3D-diagnosis, the surfaces of each halve of the craniofacial complex were compared. Moreover, the bilateral differences were statistically quantified computing the variability and significance of bilateral landmarks in UXB and control groups by PDMs and Mann-Whitney test respectively. Although a non-parametric SSM could describe the variability of the entire model, the reduced sample size would mischaracterize the transformation function leading to inaccurate results. Alternatively, PDMs identified the principal variation modes of the landmarks in both groups and the associated variability characterized. Although other morphometrics studies [31,71], in other oral disorders or congenital syndromes, have reported a relationship between the principal variation modes and some anatomical references, it was difficult to establish a clear relationship from our results. The relatively small size of our sample

or the random differences in sample selection could have affected the high dispersion level of the sample. Nevertheless, our results demonstrated the higher variability and more asymmetrical variation of the landmarks in UXB group against in the control group. In UXB group, especially remarkable was the vertical direction of the landmarks in the infraorbital and maxilla regions of the XS, whereas they varied horizontally in NXS following Trpkova et al. [72] findings.

From 3D morphological analysis, our findings revealed that the head of the condyle was wider in XS, while the condyloid process and the mandible body length were longer in NXS being in agreement with the findings of Veli et al. [41]. As a result, a sizeable gonion angle was also found in the XS as reported by Nur et al. [18]. These results provide support to the hypothesis that mandible malformations are caused due to shear and compression effects in NXS and XS mandible halves, respectively. These findings seem to support the idea that chin deviation can be used as a tool for indicating facial asymmetry. In the current research, the mandibular deviation was evaluated by two variables, ManDev and MeS (shown in Table 2), which measured the distance from the midplane of the mandible (M) or from the menton (Me) to the
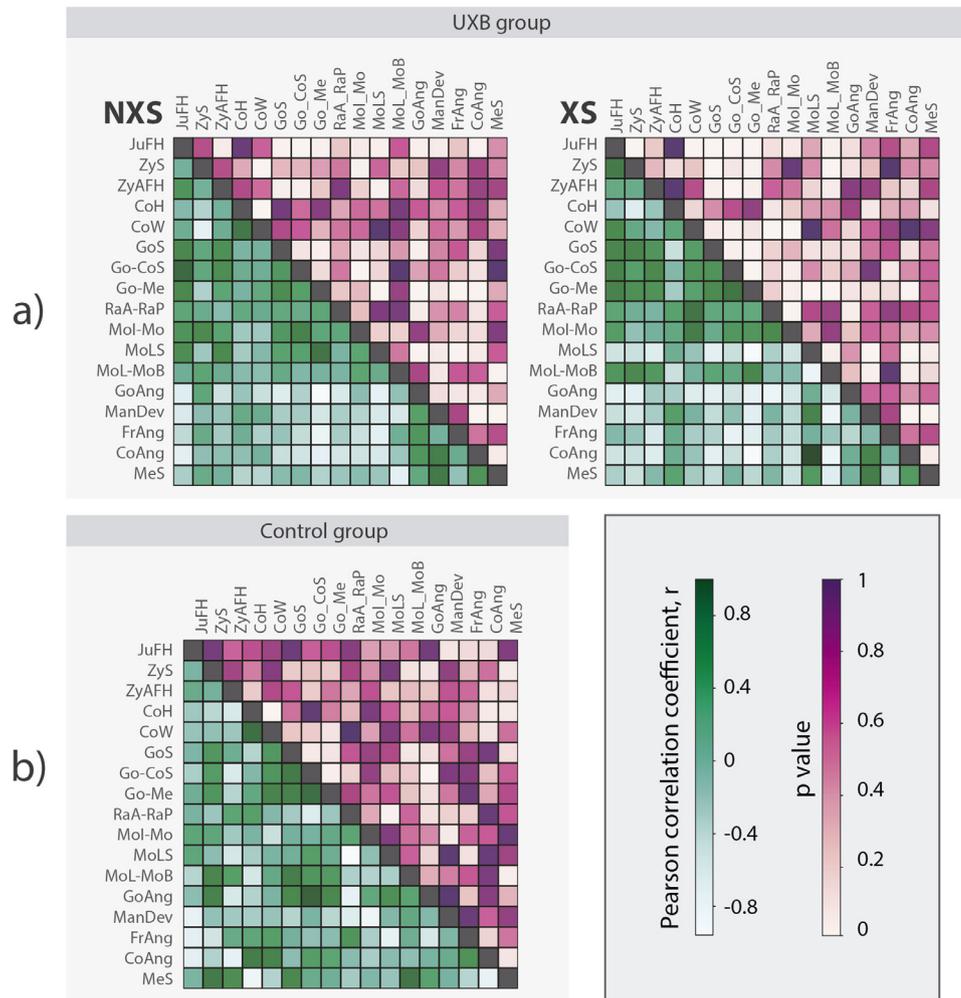
Fig. 9. Correlation matrices based on Pearson's correlation coefficient (green, below the diagonal), r, and its associated probabilistic value p (purple, above the diagonal) of the variables studied in: (a) both halves of the group of subjects with unilateral crossbite; and (b) in the control group. (For interpretation of the references to color in this figure legend, the reader is referred to the web version of this article.)

sagittal midplane. Our results suggested that the ManDev variable was more representative of the asymmetry than the MeS one. This difference may be caused because the asymmetry at early ages alters the whole shape of the mandible, but not necessarily leads to a chin displacement. This observation agrees with the conclusions of Fang et al. [73] who identified significant mandibular body deviations in patients with significant facial asymmetry despite acceptable symmetry of the mandibular contours.

Our results also reveal a morphological asymmetry of the maxilla, with the posterior maxillary region of XS being narrower than of NXS. This finding differs from those of Kwon et al. [68] who reported minor variations in the maxilla, but is broadly consistent with other clinical studies [5,43,44]. Many authors [9,74], in fact, have related breathing problems (as MBS) with UXB and facial asymmetry in accordance with Moss' functional matrix hypothesis [8], which states that nasal breathing promotes proper growth and development of the maxilla.

These results demonstrate the interrelationship between anomalies in the maxilla and its counterpart, the mandible, which was previously stated by Enlow's facial growth theory [75] and later by Kim et al. [47]. Therefore, these concurrent malformations emphasise the importance of a simultaneous assessment of maxilla and mandible. The current study found 2 groupings in subjects with moderate facial asymmetry (Fig 10b and c) that confirmed this proposition.

It is also interesting to note that malformations of the cranial base were detected in all UXB patients of this study (Fig 10b-d), with the largest effects observed in patients with severe facial asymmetry. Moreover, the differences in this region could be observed on the elevated portion of the jugale, the ocular orbit and on the narrower zygomatic arch of XS. These findings seem to be consistent with Sepahdari et al. [48] who showed an increase in cranial base and mandibular volumes on NXS.

The deviations in mandible, maxilla and cranium could be also observed in the morphological analysis of superficial soft tissues (Fig 10a-d). These results confirmed the same deviations in hard and soft tissues previously reported by Nur et al. [18] and Ryckman et al. [67], amongst others. Nevertheless, as it was aforementioned, soft tissue malformations were not statistically studied due to the high variance in paediatric patients. Our findings have therefore quantified the differences in the mandible, maxilla and skull on both sides of the face in patients with UXB and are in agreement with previous studies [5,43,44,76] and empirical theories [8,9,74,75].

4.1. Limitations

Despite the promising results of this work, some limitations need to be mentioned, such as its cross-sectional nature, i.e. different individuals with different ages and sex, which may have led to mixed results. Therefore, results should be interpreted with caution

since they could reflect random differences due to sample selection. Moreover, it might not be possible to extrapolate the findings to all patients, since the analysis has been carried with patients between 6 and 12 years old with no congenital disorders. Secondly, the size of our sample size was limited and the gender distribution in our sample was different in the control and UXB groups. Nevertheless, our sample size was based on the size of previous studies [20,52,77] which also evaluated the facial asymmetry in children by CBCT images. On the other and, the craniofacial growth differences in both genders seem not to be statistically significant [77] at ages before the puberty [78,79]. Additionally, the size differences due to gender or age variation had already been reduced after the size normalization procedure explained in Section 2.2. Nonetheless, we believe that a wider sample with equal gender distribution could result in more reliable and precise results. Future studies with a wider database could even study the shape variability of patients with facial asymmetry using SSMs. Finally, a more detailed list of anthropometric reference points could lead to new findings for the early diagnosis of facial asymmetry. We considered that 31 landmarks were enough to describe the application of this method in this computational framework. Notwithstanding this, we suggest addressing more points in further studies, especially clinical ones.

5. Conclusions

The results of this study help to elucidate the accuracy of applying computational methods in the early diagnosis of facial asymmetry providing a reliable and valuable 3D cephalometric workflow for the evaluation and quantification of asymmetrical development and planning subsequent orthodontic and surgical treatments. Within the limitations of this study, we summarize our findings by the following conclusions:

1. The PCA-based algorithm identified accurately and objectively the sagittal midplane in each subject, allowing the subsequent 3D-diagnosis workflow.
2. This 3D-method allowed to statistically demonstrate some traditional theories about the asymmetric development of the craniofacial complex in patients with UXB.
3. Morphometric analysis demonstrated greater variability and asymmetry among the patients with UXB than in the control group, requiring 8 variation modes more to define 99% of the variability.
4. The correlation analyses suggested that the degree of asymmetry could be related both with the maxillary width and mandibular deviation to the midplane identified.
5. 3D diagnosis also revealed alterations in the cranial base and soft tissues which future studies should address.

Ethical approval

The study was approved by the Research Ethics Committee of the University of São Paulo – USP, School of Dentistry (numbers 200/06 and 16/2008) and medical images was used exclusively for scientific purposes.

Funding

Declaration of Competing Interest

The authors have no conflicts of interest.

Fig. 10. Top: distance of the hard (left column) and soft (right column) tissues between the NXS region and their counterparts on XS in subjects with: (a) minor asymmetry, (b) moderate asymmetry located on the maxilla, (c) moderate asymmetry located on the mandible and (d) marked asymmetry. (e) scatter plot of ManDev global measurement and the difference of MoLS of both halves. The 3 rectangular areas divide the graph according to a pre-clinical evaluation of the degree of symmetry. The circles cluster the cases according to the obtained values of ManDev and MoLS.

Acknowledgements

Supplementary materials

Supplementary material associated with this article can be found, in the online version, at doi:10.1016/j.cmpb.2020.105397.

References

[1] C. Baek, J.Y. Paeng, J.S. Lee, J. Hong, Morphologic evaluation and classification of facial asymmetry using 3-dimensional computed tomography, J. Oral Maxillofac. Surg. 70 (2012) 1161–1169, doi:10.1016/j.joms.2011.02.135.

[2] M. Inui, K. Fushima, S. Sato, Facial asymmetry in temporomandibular joint disorders., J. Oral Rehabil. 26 (1999) 402–406, doi:10.1111/j.1365-2842.2010.02087.x.

[3] R.P. Schokker, T.L. Hansson, B.J. Ansink, L.L. Habets, Craniomandibular asymmetry in headache patients., J. Craniomandib. Disord. 4 (1990) 205–209 http://www.ncbi.nlm.nih.gov/pubmed/2098397.

[4] Y.-W. Cheong, L.-J. Lo, Facial asymmetry: etiology, evaluation, and management, Chang Gung Med. J. 34 (2014) 341–351, doi:10.1590/0103-6440201300003.

[5] P. Ngan, Contemporary orthodontics, Am. J. Orthod. Dentofac. Orthop. 142 (2012) 425, doi:10.1016/j.ajodo.2012.07.004.

[6] A. Nanci, Oral histology: development, structure, and function, J. Oral Maxillofac. Surg. 48 (1990) 98–99, doi:10.1016/0278-2391(90)90217-P.

[7] S.-J. Yoon, R.-F. Wang, H.J. Na, J.M. Palomo, Normal range of facial asymmetry in spherical coordinates: a CBCT study, Imaging Sci. Dent. 43 (2013) 31, doi:10.5624/isd.2013.43.1.31.

[8] M.L. Moss, L. Salentijn, The primary role of functional matrices in facial growth, Am. J. Orthod. 55 (1969) 566–577, doi:10.1016/0002-9416(69)90034-7.

[9] D. Harari, M. Redlich, S. Miri, T. Hamud, M. Gross, The effect of mouth breathing versus nasal breathing on dentofacial and craniofacial development in orthodontic patients, Laryngoscope 120 (2010) 2089–2093, doi:10.1002/lary.20991.

[10] N. Tsanidis, G.S. Antonarakis, S. Kiliaridis, Functional changes after early treatment of unilateral posterior cross-bite associated with mandibular shift: a systematic review, J. Oral Rehabil. 43 (2016) 59–68, doi:10.1111/joor.12335.

[11] J. Zou, M. Meng, C.S. Law, Y. Rao, X. Zhou, Common dental diseases in children and malocclusion, Int. J. Oral Sci. 10 (2018) 7, doi:10.1038/s41368-018-0012-3.

[12] L. Kurol, J. Berglund, Longitudinal study and cost-benefit analysis of the effect of early treatment of posterior cross-bites in the primary dentition, Eur. J. Orthod. 14 (1992) 173–179.

[13] P. Planas, Neuro-Occlusal Rehabilitation: NOR, Second ed., España, Amolca, Barcelona, 2013.

[14] P. Prakash, B.H. Durgesh, Anterior Crossbite Correction in Early Mixed Dentition Period Using Catlan's Appliance: A Case Report, ISRN Dent 2011 (2011) 1–5, doi:10.5402/2011/298931.

[15] L. Zhang, A. Razdan, G. Farin, J. Femiani, M. Bae, C. Lockwood, 3D face authentication and recognition based on bilateral symmetry analysis, Vis. Comput. 22 (2006) 43–55, doi:10.1007/s00371-005-0352-9.

[16] M. Pinheiro, X. Ma, M.J. Fagan, G.T. McIntyre, P. Lin, G. Sivamurthy, P.A. Mossey, A 3D cephalometric protocol for the accurate quantification of the craniofacial symmetry and facial growth, J. Biol. Eng. 13 (2019) 42, doi:10.1186/s13036-019-0171-6.

[17] R. Nanda, M.J. Margolis, Treatment strategies for midline discrepancies, Semin. Orthod. 2 (1996) 84–89, doi:10.1016/S1073-8746(96)80046-6.

[18] R.B. Nur, D.G. Çakan, T. Arun, Evaluation of facial hard and soft tissue asymmetry using cone-beam computed tomography, Am. J. Orthod. Dentofac. Orthop. 149 (2016) 225–237, doi:10.1016/j.ajodo.2015.07.038.

[19] P. Berssenbrügge, N.F. Berlin, G. Kebeck, C. Runte, S. Jung, J. Kleinheinz, D. Dirksen, 2D and 3D analysis methods of facial asymmetry in comparison, J, Cranio-Maxillofacial Surg 42 (2014) e327–e334, doi:10.1016/j.jcms.2014.01.028.

[20] E. Huntjens, G. Kiss, C. Wouters, C. Carels, Condylar asymmetry in children with juvenile idiopathic arthritis assessed by cone-beam computed tomography, Eur. J. Orthod. 30 (2008) 545–551, doi:10.1093/ejo/cjn056.

[21] J. Damstra, Z. Fourie, M. De Wit, Y. Ren, A three-dimensional comparison of a morphometric and conventional cephalometric midsagittal planes for craniofacial asymmetry, Clin. Oral Investig. 16 (2012) 285–294, doi:10.1007/s00784-011-0512-4.

[22] S.M. Shin, Y.-M.Y.-I. Kim, N.-R. Kim, Y.-S. Choi, S.-B. Park, Y.-M.Y.-I. Kim, Statistical shape analysis-based determination of optimal midsagittal reference plane for evaluation of facial asymmetry, Am. J. Orthod. Dentofac. Orthop. 150 (2016) 252–260, doi:10.1016/j.ajodo.2016.01.017.

[23] A. Dobai, Z. Markella, T. Vízkelety, C. Fouquet, A. Rosta, J. Barabás, Landmark-based midsagittal plane analysis in patients with facial symmetry and asymmetry based on CBCT analysis tomography, J. Orofac. Orthop. / Fortschritte Der Kieferorthopädie. 79 (2018) 371–379, doi:10.1007/s00056-018-0151-3.

[24] H.-J. Kim, B.C. Kim, J.-G. Kim, P. Zhengguo, S.H. Kang, S.-H. Lee, Construction and validation of the midsagittal reference plane based on the skull base symmetry for three-dimensional cephalometric craniofacial analysis, J. Craniofac. Surg. 25 (2014) 338–342, doi:10.1097/SCS.0000000000000380.

[25] A. Katsumata, M. Fujishita, M. Maeda, Y. Ariji, E. Ariji, R.P. Langlais, 3D-CT evaluation of facial asymmetry, Oral Surg. Oral Med. Oral Pathol. Oral Radiol. Endodontol. 99 (2005) 212–220, doi:10.1016/j.tripleo.2004.06.072.

[26] T.-Y. Kim, J.-S. Baik, J.-Y. Park, H.-S. Chae, K.-H. Huh, S.-C. Choi, Determination of midsagittal plane for evaluation of facial asymmetry using three-dimensional computed tomography, Imaging Sci. Dent. 41 (2011) 79, doi:10.5624/isd.2011.41.2.79.

[27] A. Gong, J. Li, Z. Wang, Y. Li, F. Hu, Q. Li, D. Miao, L. Wang, Cranial base characteristics in anteroposterior malocclusions: a meta-analysis, Angle Orthod. 86 (2016) 668–680, doi:10.2319/032315-186.1.

[28] A.B. Lipira, S. Gordon, T.A. Darvann, N.V. Hermann, A.E. Van Pelt, S.D. Naidoo, D. Govier, A.A. Kane, Helmet versus active repositioning for plagiocephaly: a three-dimensional analysis, Pediatrics 126 (2010) e936–e945, doi:10.1542/peds.2009-1249.

[29] S. Lanche, T.A. Darvann, H. Ólafsdóttir, N.V Hermann, A.E. Van Pelt, D. Govier, M.J. Tenenbaum, S. Naidoo, P. Larsen, S. Kreiborg, A statistical model of head asymmetry in infants with deformational plagiocephaly, in: Scand. Conf. Image Anal., Springer, 2007, pp. 898–907.

[30] M.-J. Cho, R.R. Hallac, J. Ramesh, J.R. Seaward, N.V. Hermann, T.A. Darvann, A. Lipira, A.A. Kane, Quantifying normal craniofacial form and baseline craniofacial asymmetry in the pediatric population, Plast. Reconstr. Surg. 141 (2018) 380e–387e, doi:10.1097/PRS.0000000000004114.

[31] S.C. Schaal, C. Ruff, B.I. Pluijmers, E. Pauws, C.W.N. Looman, M.J. Koudstaal, D.J. Dunaway, Characterizing the skull base in craniofacial microsomia using principal component analysis, Int. J. Oral Maxillofac. Surg. 46 (2017) 1656–1663, doi:10.1016/j.ijom.2017.07.008.

[32] B.D.P.J. Maas, B.I. Pluijmers, P.G.M. Knoops, C. Ruff, M.J. Koudstaal, D. Dunaway, Using principal component analysis to describe the midfacial deformities in patients with craniofacial microsomia, J. Cranio-Maxillofacial Surg. 46 (2018) 2032–2041, doi:10.1016/j.jcms.2018.09.019.

[33] T.F. Cootes, C.J. TaylorM. Sonka, K.M. Hanson (Eds.), Statistical models of appearance for medical image analysis and computer vision, N. Engl. J. Med. (2001) 236–248, doi:10.1117/12.431093.

[34] W. Semper-Hogg, M.A. Fuessinger, S. Schwarz, E. Ellis, C.-P. Cornelius, F. Probst, M.C. Metzger, S. Schlager, Virtual reconstruction of midface defects using statistical shape models, J. Cranio-Maxillofacial Surg 45 (2017) 461–466, doi:10.1016/j.jcms.2016.12.020.

[35] M.A. Fuessinger, S. Schwarz, C.-P. Cornelius, M.C. Metzger, E. Ellis, F. Probst, W. Semper-Hogg, M. Gass, S. Schlager, Planning of skull reconstruction based on a statistical shape model combined with geometric morphometrics, Int. J. Comput. Assist. Radiol. Surg. 13 (2018) 519–529, doi:10.1007/s11548-017-1674-6.

[36] P. Mitteroecker, P. Gunz, Advances in Geometric Morphometrics, Evol. Biol. 36 (2009) 235–247, doi:10.1007/s11692-009-9055-x.

[37] A. Dall'Asta, S. Schievano, J.L. Bruse, G. Paramasivam, C.T. Kaihura, D. Dunaway, C.C. Lees, Quantitative analysis of fetal facial morphology using 3D ultrasound and statistical shape modeling: a feasibility study, Am. J. Obstet. Gynecol. 217 (2017) 76.e1–76.e8, doi:10.1016/j.ajog.2017.02.007.

[38] J.L. Bruse, K. McLeod, G. Biglino, H.N. Ntsinjana, C. Capelli, T.-Y. Hsia, M. Sermesant, X. Pennec, A.M. Taylor, S. Schievano, A statistical shape modelling framework to extract 3D shape biomarkers from medical imaging data: assessing arch morphology of repaired coarctation of the aorta, BMC Med. Imaging. 16 (2016) 40, doi:10.1186/s12880-016-0142-z.

[39] N. Sarkalkan, H. Weinans, A.A. Zadpoor, Statistical shape and appearance models of bones, Bone 60 (2014) 129–140, doi:10.1016/j.bone.2013.12.006.

[40] S. Durrleman, X. Pennec, A. Trouvé, N. Ayache, Measuring brain variability via sulcal lines registration: a diffeomorphic approach, in: Med. Image Comput. Comput. Interv. – MICCAI 2007, Springer Berlin Heidelberg, Berlin, Heidelberg, n.d.: pp. 675–682. doi:10.1007/978-3-540-75757-3_82.

[41] I. Veli, T. Uysal, T. Ozer, F.I. Ucar, M. Eruz, Mandibular asymmetry in unilateral and bilateral posterior crossbite patients using cone-beam computed tomography, Angle Orthod. 81 (2011) 966–974, doi:10.2319/022011-122.1.

[42] P. Pirttiniemi, T. Kantomaa, P. Lahtela, Relationship between craniofacial and condyle path asymmetry in unilateral cross-bite patients, Eur. J. Orthod. 12 (1990) 408–413, doi:10.1093/ejo/12.4.408.

[43] C.A. Wong, P.M. Sinclair, R.G. Keim, D.B. Kennedy, Arch dimension changes from successful slow maxillary expansion of unilateral posterior crossbite, Angle Orthod 81 (2011) 616–623, doi:10.2319/072210-429.1.

[44] F. Ferro, P. Spinella, N. Lama, Transverse maxillary arch form and mandibular asymmetry in patients with posterior unilateral crossbite, Am. J. Orthod. Dentofac. Orthop. 140 (2011) 828–838, doi:10.1016/j.ajodo.2011.08.003.

[45] V. Katyal, Y. Pamula, C.N. Daynes, J. Martin, C.W. Dreyer, D. Kennedy, W.J. Sampson, Craniofacial and upper airway morphology in pediatric sleep-disordered breathing and changes in quality of life with rapid maxillary expansion, Am. J. Orthod. Dentofac. Orthop. 144 (2013) 860–871, doi:10.1016/j.ajodo.2013.08.015.

[46] H. Kapadia, P.R. Shetye, B.H. Grayson, J.G. McCarthy, Cephalometric assessment of craniofacial morphology in patients with treacher Collins syndrome., J. Craniofac. Surg. 24 (2013) 1141–1145, doi:10.1097/SCS.0b013e3182860541.

[47] S.-J. Kim, K.-J. Lee, S.-H. Lee, H.-S. Baik, Morphologic relationship between the cranial base and the mandible in patients with facial asymmetry and mandibular prognathism, Am. J. Orthod. Dentofacial Orthop. 144 (2013) 330–340, doi:10.1016/j.ajodo.2013.03.024.

[48] A.R. Sepahdari, S. Mong, Skull base CT: normative values for size and symmetry of the facial nerve canal, foramen ovale, pterygoid canal, and foramen rotundum, Surg. Radiol. Anat. 35 (2013) 19–24, doi:10.1007/s00276-012-1001-4.

[49] S. Hara, M. Mitsugi, T. Kanno, A. Nomachi, T. Wajima, Y. Tatemoto, Three-dimensional virtual operations can facilitate complicated surgical planning for the treatment of patients with jaw deformities associated with facial asymmetry: a case report, Int. J. Oral Sci. 5 (2013) 176–182, doi:10.1038/ijos.2013.48.

[50] I. Saitoh, C. Yamada, H. Hayasaki, T. Maruyama, Y. Iwase, Y. Yamasaki, Is the reverse cycle during chewing abnormal in children with primary dentition? J. Oral Rehabil 37 (2010) 26–33, doi:10.1111/j.1365-2842.2009.02006.x.

[51] L. Sonnesen, M. Bakke, Bite force in children with unilateral crossbite before and after orthodontic treatment. A prospective longitudinal study, Eur. J. Orthod. 29 (2007) 310–313, doi:10.1093/ejo/cjl082.

[52] E. Illipronti-Filho, S.M. de Fantini, I. Chilvarquer, Evaluation of mandibular condyles in children with unilateral posterior crossbite, Braz. Oral Res. 29 (2015) 49, doi:10.1590/1807-3107BOR-2015.vol29.0049.

[53] Y. Wang, S. He, L. Yu, J. Li, S. Chen, Accuracy of volumetric measurement of teeth in vivo based on cone beam computer tomography, Orthod. Craniofac. Res. 14 (2011) 206–212, doi:10.1111/j.1601-6343.2011.01525.x.

[54] H. Lin, P. Zhu, Y. Lin, S. Wan, X. Shu, Y. Xu, Y. Zheng, Mandibular asymmetry: A three-dimensional quantification of bilateral condyles, Head Face Med 9 (2013) 1–7, doi:10.1186/1746-160x-9-42.

[55] L. Keilig, M. Drolshagen, K.L. Tran, I. Hasan, S. Reimann, J. Deschner, K.T. Brinkmann, R. Krause, M. Favino, C. Bourauel, In vivo measurements and numerical analysis of the biomechanical characteristics of the human periodontal ligament, Ann. Anat. - Anat. Anzeiger. 206 (2016) 80–88, doi:10.1016/j.aanat.2015.08.004.

[56] B. Xu, Y. Wang, Q. Li, Modeling of damage driven fracture failure of fiber post-restored teeth, J. Mech. Behav. Biomed. Mater. 49 (2015) 277–289, doi:10.1016/j.jmbbm.2015.05.006.

[57] J.C. Gower, Generalized procrustes analysis, Psychometrika 40 (1975) 33–51, doi:10.1007/BF02291478.

[58] J. O'Rourke, Finding minimal enclosing boxes, Int. J. Comput. Inf. Sci. 14 (1985) 183–199, doi:10.1007/BF00991005.

[59] J. Damstra, B.C.M. Oosterkamp, J. Jansma, Y. Ren, Combined 3-dimensional and mirror-image analysis for the diagnosis of asymmetry, Am. J. Orthod. Dentofac. Orthop. 140 (2011) 886–894, doi:10.1016/j.ajodo.2010.03.032.

[60] P.J. Besl, N.D. McKay, Method for registration of 3-D shapes, in: P.S. Schenker (Ed.), Sens. Fusion IV Control Paradig. Data Struct., International Society for Optics and Photonics, 1992, pp. 586–606, doi:10.1117/12.57955.

[61] D. Lonic, A. Sundoro, H.-H. Lin, P.-J. Lin, L.-J. Lo, Selection of a horizontal reference plane in 3D evaluation: identifying facial asymmetry and occlusal cant in orthognathic surgery planning, Sci. Rep. 7 (2017) 2157, doi:10.1038/s41598-017-02250-w.

[62] J. Alabort-i-Medina, E. Antonakos, J. Booth, P. Snape, S. Zafeiriou, Menpo, in: Proc. ACM Int. Conf. Multimed. - MM '14, New York, New York, USA, ACM Press, 2014, pp. 679–682, doi:10.1145/2647868.2654890.

[63] B.F. Gribel, M.N. Gribel, D.C. Frazão, J.A. McNamara Jr, F.R. Manzi, Accuracy and reliability of craniometric measurements on lateral cephalometry and 3D measurements on CBCT scans, Angle Orthod. 81 (2011) 26–35.

[64] G. Akhil, K. Senthil Kumar, S. Raja, K. Janardhanan, Three-dimensional assessment of facial asymmetry: a systematic review, J. Pharm. Bioallied Sci. 7 (2015) 433, doi:10.4103/0975-7406.163491.

[65] N. Zamora, J.M. Llamas, R. Cibrián, J.L. Gandia, V. Paredes, Cephalometric measurements from 3D reconstructed images compared with conventional 2D images, Angle Orthod. 81 (2011) 856–864, doi:10.2319/121210-717.1.

[66] P. Pittayapat, M.M. Bornstein, T.S.N. Imada, W. Coucke, I. Lambrichts, R. Jacobs, Accuracy of linear measurements using three imaging modalities: two lateral cephalograms and one 3D model from CBCT data, Eur. J. Orthod. 37 (2015) 202–208, doi:10.1093/ejo/cju036.

[67] M.S. Ryckman, S. Harrison, D. Oliver, C. Sander, A.A. Boryor, A.A. Hohmann, F. Kilic, K.B. Kim, Soft-tissue changes after maxillomandibular advancement surgery assessed with cone-beam computed tomography, Am. J. Orthod. Dentofac. Orthop. 137 (2010) S86–S93, doi:10.1016/j.ajodo.2009.03.041.

[68] T.G. Kwon, H.S. Park, H.M. Ryoo, S.H. Lee, A comparison of craniofacial morphology in patients with and without facial asymmetry - A three-dimensional analysis with computed tomography, Int. J. Oral Maxillofac. Surg. 35 (2006) 43–48, doi:10.1016/j.ijom.2005.04.006.

[69] P.M. Pirttiniemi, Associations of mandibular and facial asymmetries—A review, Am. J. Orthod. Dentofac. Orthop. 106 (1994) 191–200, doi:10.1016/S0889-5406(94)70038-9.

[70] R.C. Solem, A. Ruellas, A. Miller, K. Kelly, J.L. Ricks-Oddie, L. Cevidanes, Congenital and acquired mandibular asymmetry: Mapping growth and remodeling in 3 dimensions, Am. J. Orthod. Dentofacial Orthop. 150 (2016) 238–251, doi:10.1016/j.ajodo.2016.02.015.

[71] G. Laganà, V. Di Fazio, V. Paoloni, L. Franchi, P. Cozza, R. Lione, Geometric morphometric analysis of the palatal morphology in growing subjects with skeletal open bite, Eur. J. Orthod. 41 (2019) 258–263, doi:10.1093/ejo/cjy055.

[72] B. Trpkova, N.G. Prasad, E.W.N. Lam, D. Raboud, K.E. Glover, P.W. Major, Assessment of facial asymmetries from posteroanterior cephalograms: validity of reference lines, Am. J. Orthod. Dentofac. Orthop. 123 (2003) 512–520, doi:10.1016/S0889-5406(02)57034-7.

[73] J.-J. Fang, Y.-H. Tu, T.-Y. Wong, J.-K. Liu, Y.-X. Zhang, I.-F. Leong, K.-C. Chen, Evaluation of mandibular contour in patients with significant facial asymmetry, Int. J. Oral Maxillofac. Surg. 45 (2016) 922–931, doi:10.1016/j.ijom.2016.02.008.

[74] C.E. Zambon, M.M. Ceccheti, E.R. Utumi, F.R. Pinna, G.G. Machado, M.P.S.M. Peres, R.L. Voegels, Orthodontic measurements and nasal respiratory function after surgically assisted rapid maxillary expansion: an acoustic rhinometry and rhinomanometry study, Int. J. Oral Maxillofac. Surg. 41 (2012) 1120–1126, doi:10.1016/j.ijom.2011.12.037.

[75] D.H. Enlow, Facial growth, WB Saunders Company, 1990.

[76] M.Y. Leung, Y.Y. Leung, Three-dimensional evaluation of mandibular asymmetry: a new classification and three-dimensional cephalometric analysis, Int. J. Oral Maxillofac. Surg. 47 (2018) 1043–1051, doi:10.1016/j.ijom.2018.03.021.

[77] L. Abad-Santamaría, A. López-de-Andrés, I. Jiménez-Trujillo, C. Ruíz, M. Romero, Effect of unilateral posterior crossbite and unilateral cleft lip and palate on vertical mandibular asymmetry, Ir. J. Med. Sci. 183 (2014) 357–362, doi:10.1007/s11845-013-1020-0.

[78] H.S. Matthews, A.J. Penington, R. Hardiman, Y. Fan, J.G. Clement, N.M. Kilpatrick, P.D. Claes, Modelling 3D craniofacial growth trajectories for population comparison and classification illustrated using sex-differences, Sci. Rep. 8 (2018) 4771, doi:10.1038/s41598-018-22752-5.

[79] S. Pirinen, Endocrine regulation of craniofacial growth, Acta Odontol. Scand. 53 (1995) 179–185, doi:10.3109/00016359509005969.